Amplification of molecular traffic control in catalytic grains with novel channel topology design

Andreas Brzank[a)]
Institut für Festkörperforschung, Forschungszentrum Jülich, 52425 Jülich, Germany and Fakultät für Physik und Geowissenchaften, Universität Leipzig, Abteilung Grenzflächenphysik, Linnestrasse 5, D-04103 Leipzig, Germany

Gunter M. Schütz
Institut für Festkörperforschung, Forschungszentrum Jülich, 52425 Jülich, Germany

(Received 30 December 2005; accepted 6 April 2006; published online 1 June 2006)

We investigate the conditions for reactivity enhancement of catalytic processes in porous solids by the use of molecular traffic control (MTC). With dynamic Monte-Carlo simulations and continuous-time master equation theory applied to the high concentration regime, we obtain a quantitative description of the MTC effect for a network of intersecting single-file channels in a wide range of grain parameters and for optimal external operating conditions. Implementing the concept of MTC in models with specially designed alternating bimodal channels, we find the efficiency ratio (compared with a topologically and structurally similar reference system without MTC) to be enhanced with increasing grain diameter, a property verified for the first time for a MTC system. Even for short intersection channels, MTC leads to a reactivity enhancement of up to approximately 65%. This suggests that MTC may significantly enhance the efficiency of a catalytic process for small as well as large porous particles with a suitably chosen binary channel topology.
 [DOI: 10.1063/1.2200691]

I. INTRODUCTION

Zeolites are used for catalytic processes in a variety of applications, e.g., cracking of large hydrocarbon molecules. In a number of zeolites diffusive transport occurs along quasi-one-dimensional channels which do not allow guest molecules to pass each other.[1] Due to mutual blockage of reactants A and product molecules B under such *single-file conditions*[2] the effective reactivity of a catalytic process $A \rightarrow B$—determined by the residence time of molecules in the zeolite—may be considerably reduced as compared to the reactivity in the absence of single-file behavior. It has been suggested that the single-file effect may be circumvented by the concept of molecular traffic control[3,4] (MTC) which has remained controversial for a long time. This notion rests on the assumption that reactants and product molecules, respectively, may prefer spatially separated diffusion pathways and thus avoid mutual suppression of self-diffusion inside the grain channels.

The necessary (but not sufficient) requirement for the MTC effect, a channel selectivity of two different species of molecules, has been verified by means of molecular dynamics (MD) simulations of two-component mixtures in the zeolite ZSM-5 (Ref. 5) and relaxation simulations of a mixture of differently sized molecules (Xe and SF_6) in a bimodal structure possessing dual-sized pores (Boggsite with 10-ring and 12-ring pores).[6] Also equilibrium Monte-Carlo simulations demonstrate that the residence probability in different areas of the intracrystalline pore space may be notably different for the two components of a binary mixture[7] and thus provide further support for the notion of channel selectivity in suitable bimodal channel topologies.

Whether an MTC effect leading to reactivity enhancement actually takes place was addressed in a series of dynamic Monte Carlo simulations (DMCS) of a stochastic model system with a network of perpendicular sets of bimodal intersecting channels and with catalytic sites located at the intersecting pores [NBK model Fig. 1(b)].[8–10,13,14] The authors of these studies found numerically the occurrence of the MTC effect by comparing the outflow of reaction products in the MTC system with the outflow from a reference system [REF model Fig. 1(a)] with equal internal and external system parameters, as well as equal internal and optimal external system parameters. The dependency of the MTC effect as a function of the system size and catalytic reactivity has been investigated in Refs. 11 and 13. The MTC effect is favored by a small number of channels and long channels between intersections, which by themselves lead to a very low absolute outflow compared to a similar system with shorter channels. For reasonable reactivities and channel lengths the MTC effect vanishes inversely proportional to the grain diameter. An analytical treatment of the master equation for this stochastic many-particle model revealed the origin of this effect at high reactivities.[12] It results from an interplay of the long residence time of guest molecules under single-file conditions with a saturation effect that leads to a depletion of the bulk of the crystallite. The extension of the NBK model to three dimensions[14] leads to similar results with the conclusion that MTC may enhance significantly the effective reactivity in zeolitic nanoparticles with suitable bi-

a)Electronic mail: a.brzank@fz-juelich.de

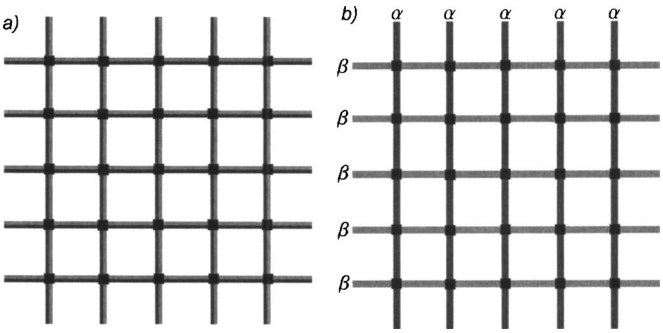

FIG. 1. REF system (a), NBK model consisting of perpendicular α/β channels (b)—both with channel number of $N=5$. In contrast to the REF case, where we allow both types of particles (A and B particles) to enter any channel, in the MTC system A particles are carried through the α channels whereas the B particles diffuse along the β channels. Black squares indicate catalytic sites where a catalytic transition $A \rightarrow B$ takes place.

nary channel systems and thus may be of practical relevance in applications. However, no MTC effect with sufficient absolute effective reactivity can be expected with NBK channel topology for large grains of at present commercially used size.

Here we address this question by investigating the MTC effect for a novel channel topology (Fig. 2) consisting of alternating α and β channels. With a view on applications we focus on small channel length. Moreover, for the same reason we determine the MTC effect by making a comparison with the reference system using the same set of fixed internal (material-dependent) parameters, but (unlike in previous studies[10–12]) for each case (MTC and REF, respectively) different optimal external (operation-dependent) parameters which one would try to implement in an industrially relevant process. This may be of interest as since the first successful synthesis of mesoporous MCM-41 nanoparticles[15] there has been intense research activity in the design and synthesis of structured mesoporous solids with a controlled pore size. In particular, synthesis of bimodal nanostructures with independently controlled small and large mesopore sizes has become feasible.[16] It will transpire that a significant MTC effect (reactivity enhancement up to 65%) occurs in our model system even for small channel length at realistic intermediate reaction rates of the catalyst.

II. THE MODEL

We consider a lattice model with a quadratic array of $N \times N$ channels (Fig. 2) which is a measure of the grain size of the crystallite. Each channel has L sites between the intersection points where the irreversible catalytic process $A \rightarrow B$ takes place. We assume the boundary channels of the grain to be connected to the surrounding gas phase, modeled by extra reservoir sites of constant A particle density ρ. We assume the reaction products B which leave the crystallite to be removed immediately from the gas phase such that the density of product particles in the reservoir is always 0. Short-range interaction between particles inside the narrow pores is described by an idealized hard-core repulsion which forbids double occupancy of lattice sites. The state space is finite and the state of a single lattice site i is represented by

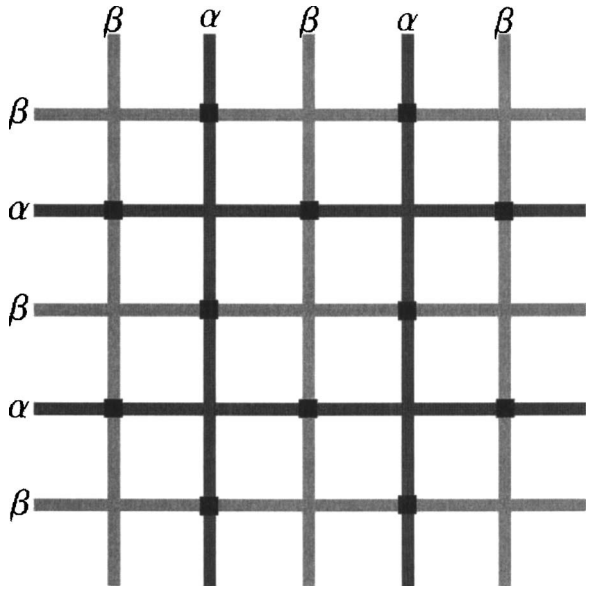

FIG. 2. MTC system with alternating α/β channels ($N=5$). Black squares indicate catalytic sites where a catalytic transition $A \rightarrow B$ takes place.

the particle numbers $a_i=0$, 1 and $b_i=0,1$ corresponding to having an A ($a_i=1$, $b_i=0$), B ($b_i=1$, $a_i=0$) or no particle ($a_i=b_i=0$) at site i. The density profile of the system is determined by the expectation values of the particle numbers. Particles have unit mass and a lattice site represents unit volume inside the channel system. Therefore $\rho(i)$ in our model is a dimensionless quantity, taking values between 0 and 1.

The underlying dynamics are stochastic. We work in a continuous-time description where the transition probabilities become transition rates and no multiple transitions occur at the same infinitesimal time unit. Each elementary transition between microscopic configurations of the system takes place randomly with an exponential waiting-time distribution. Diffusion is modeled by jump processes between neighboring lattice sites. D is the elementary (attempt) rate of hopping and is assumed to be the same for both species A, B of particles. In the absence of other particles D is the self-diffusion coefficient for the mean-square displacement along a channel. Recalling the lattice unit one, D has the dimension one over time unit. If a neighboring site is occupied by a particle, then a hopping attempt is rejected (single-file effect). The dynamics inside a channel are thus given by the symmetric exclusion process[17–20] which is well studied in the probabilistic[21] and statistical mechanics literature.[22] The self-diffusion along a channel is anomalous, the effective diffusion rate between intersection points decays asymptotically as $1/L$, see Ref. 19 and references therein.

At the intersections the reaction $A \rightarrow B$ occurs with a reaction rate c which is the reaction probability per unit time. This reaction rate influences, but is distinct from, the effective grain reactivity which is largely determined by the residence time of guest molecules inside the grain which under single-file conditions grows in the reference system with the third power of the channel length L.[23] At the boundary sites, particles jump into the reservoir with a rate $D(1-\rho_A-\rho_B)$ in

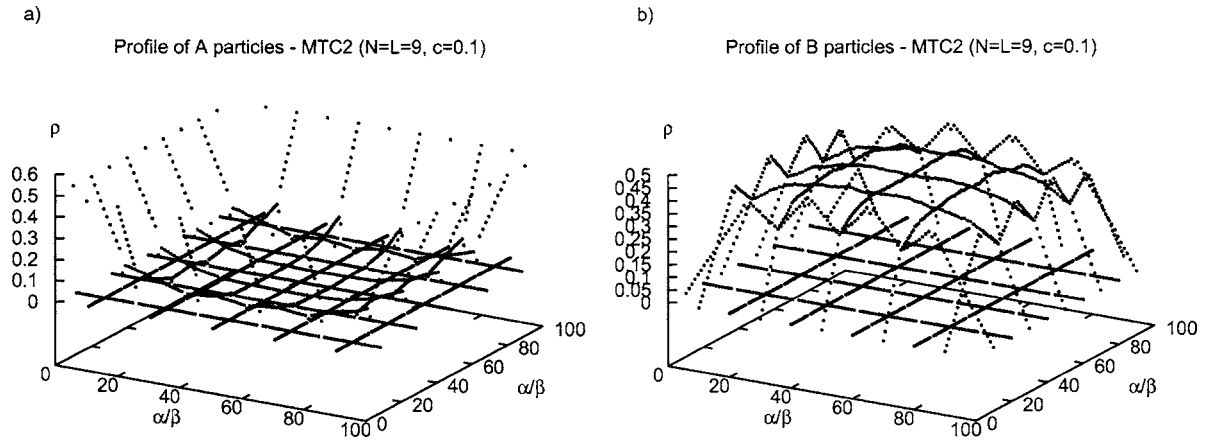

FIG. 3. A/B particle profile (a)/(b) for the MTC system of $N=L=9$ and reactivity $c=0.1$.

the general case. Correspondingly, particles are injected into the grain with rates $D\rho_{A,B}$ respectively. As discussed above here we consider only $\rho_A=\rho$, $\rho_B=0$.

For the REF system reactants as well as product particles are allowed to enter and leave both types of channels. In the case of MTC reactant(product) particles will enter $\alpha(\beta)$ channels only, mimicking complete channel selectivity. Therefore all channel segments carry only one type of particles in the MTC case. For the boundary channels complete selectivity implies that α channels are effectively described by connection with an A reservoir of density $\rho_A=\rho$ (particles of type B do not block the boundary sites of α channels) and β channels are effectively described by connection with a B reservoir of density $\rho_B=0$, respectively (particles of type A do not block the boundary sites of β-channels). This stochastic dynamics, which is a Markov process, fully defines our MTC model.

In both cases, MTC and REF, the external concentration gradient between reactant and product reservoir densities induces a particle current inside the grain which drives the system in a stationary nonequilibrium state. For this reason there is no Gibbs measure and equilibrium Monte-Carlo algorithms cannot be applied for determining steady-state properties. Instead we use dynamic Monte Carlo simulation (DMCS) with random sequential update. This ensures that the simulation algorithm yields the correct stationary distribution of the model.

III. MONTE CARLO RESULTS

Anticipating concentration gradients between intersection points, we expect, due to the exclusion dynamics linear density profiles within the channel segments,[12,18,22] the slope and hence the current to be inversely proportional to the number of lattice sites L. The total output current j of the product particles, defined as the number of B particles leaving the grain per time unit in the stationary state, is the main quantity of interest and has unit one over time unit. It determines the effective reactivity of the grain.

Figure 3 shows the particle densities for the reactants (a) and product particles (b) in the stationary regime for the MTC system $N=L=9$ and reactivity $c=0.1$. Every other boundary-channel segment contributes to the output; therefore we expect no efficiency loss with increasing N. We are particularly interested in studying the system in its maximal current state for given reactivity c and size constants N, L, which are intrinsic material properties of the grain. The reactant particle reservoir density ρ, determined by the density in the gas phase, can be tuned in a possible experimental setting. Let us therefore denote the reservoir density which maximizes the output current with ρ^* and the maximal current with j^*. We iteratively approach the maximal current by a set of nine data points. Figure 4 shows j as a function of ρ for both MTC and REF systems of $N=5$, $L=1$ and reactivity $c=0.01$. The "best" datapoint has been chosen in order to approximate the maximum. Statistical errors are displayed; they are, however, mostly within, symbol size. We note that for the MTC system the maximal current is attuned for $\rho^*=1$. REF and MTC systems show a similar dependence of the maximal current as a function of the reactivity (Fig. 5). In contrast to the NBK topology,[13] $j^*(c)$ is a monotonically increasing function and the highest product particle output is achieved for infinite reactivity. In this case any transition $A\rightarrow B$ transpires close to the surface and hence, from an applied point of view one would be interested in various small grains rather than view big ones.

In order to measure the efficiency of a MTC system over the associated REF system we define the efficiency ratio

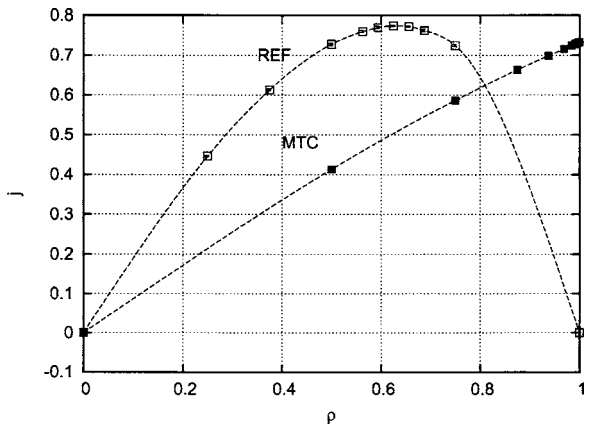

FIG. 4. j_{MTC} (solid symbols) and j_{REF} (open symbols) as a function of the reservoir density for a system with $N=5$, $L=1$ and $c=0.1$.

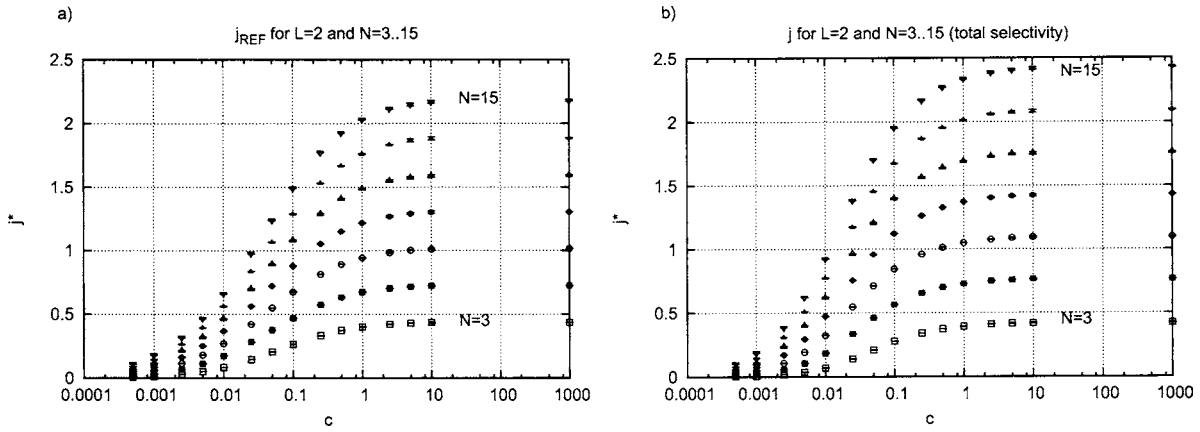

FIG. 5. Maximal currents j^* over reactivity c for the REF system (a) and MTC system (b) for different N.

$$R(c,N,L) = \frac{j^*_{\mathrm{MTC}}}{j^*_{\mathrm{REF}}}, \tag{1}$$

which is a function of the system size N, L and reactivity c.

Figure 6(a) shows the measured ratio R for a large range of reactivities. We plotted systems with $L=2$ and different N. We find an MTC effect over a large range of reactivities. There is a small tendency of growing efficiency with increasing N. This is highly desirable since an enhancement of efficiency due to MTC is thus not restricted to nanoscale crystallites. Compared to former studies of MTC systems, this is a qualitatively new property and results from the fact that the number of output (β channels) scales linearly with growing system size N. In general, compared to the NBK model, the efficiency ratio remains quite unchanged in the regime of simulated reactivities. There is no sharp decrease for large reactivities. Nevertheless, we notice an optimal reactivity c^* for which R becomes maximal. This value is denoted by R^* and plotted in Fig. 6(b) for increasing N and different L. The MTC effect is present for any L and our model exhibits an enhancement of the effective reactivity of up to 20% for (extremely) short channel length ($L=1$) and up to 65% for $L=3$.

As expected from previous results [11,12] the MTC effect is seen to increase with increasing L (Fig. 7). This follows from theoretical studies of single-file systems which predict that the mean traveling time of a product molecule through a channel of length L is proportional to L^2 in the MTC case as in ordinary diffusion, but proportional to L^3 in the REF case due to mutual blockage. Hence the current is proportional to $1/L$ in a MTC system, but proportional to $1/L^2$ in a REF system. This holds for all values of the parameters and hence, for sufficiently large L, the MTC system becomes more efficient.

IV. THE HIGH-REACTIVITY CASE

The penetration depth of reactant particles into the system is related to the reactivity c. In the fast-reactivity case transitions and particle transport take place close to the grain surface. Figure 8 shows the profile of the reactant particles (a) and product particles (b) for a system of $N=9$ channels, $L=15$ and fast reactivity ($c=1000$). Notice that almost no reactants reach the bulk of the system since reactants entering the system are converted very likely into product particles at the first intersection. Hence, a creation of product particles occurs only on the outer β channels, which leads to the equilibration of the product particles in the bulk of the system. This picture is supported by simulation (Fig. 8) and suggests defining a reduced system, illustrated in Fig. 9, for the following theoretical analysis. We already included the symmetry of the problem in the notation of Fig. 9.

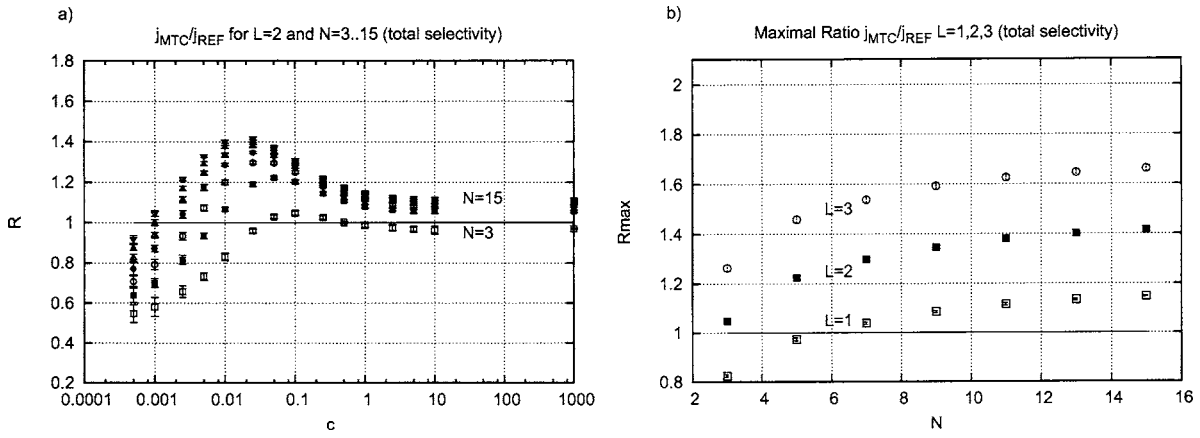

FIG. 6. (a) Ratio $R(c)$ for different number of channels N and $L=2$. (b) Maximal ratio R^* for different L.

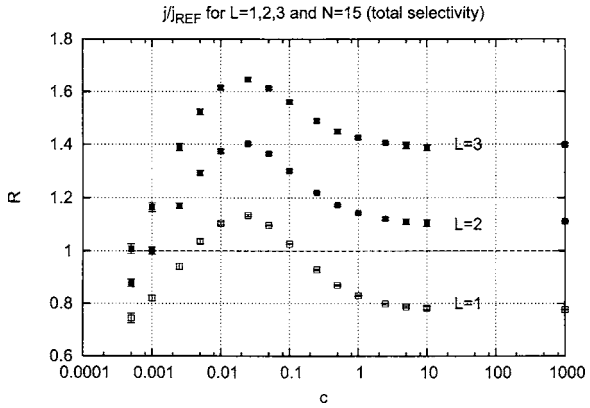

FIG. 7. Dependence of the output ratio on the channel length L.

Here, α segments carrying no particles are suppressed, β segments in equilibrium are represented by dotted lines. The density profile in a channel segment enclosed by two intersections or an intersection and boundary site is linear due to pure exclusion dynamics.[20] This allows us to reduce our effort to the computation of the intersection densities. The strategy is, as in Ref. 12, to obtain a recursion relation for the intersection B particle densities. Single-file diffusion within the channels can be described by a single-species master equation[22] which in the stationary state gives a set of equations containing only second order differences of single-site densities. Any joint probability vanishes in the bulk of the channels.[20] Only intersection sites and their three neighbors involve product expectation values of the form $\langle a_i b_{i+1}\rangle$. Within a mean field approximation, joint probabilities can be replaced by the product of the individual averages $\langle a_i\rangle\langle b_{i+1}\rangle$. This well controlled approximation is, in fact, necessary only in the vicinity of intersections. The expected relative error is of the order of $1/L$.[18,22] This provides a closed set of equations for single-site densities. One could reduce the complexity by identifying the currents for the different channel segments and taking into account the conservation of currents at the intersection. The output of product particles, i.e., the number of B's leaving the system, is given by the currents j_x^B of the β segments connected to the reservoir. The calculation is similar to Ref. 12 and we identify

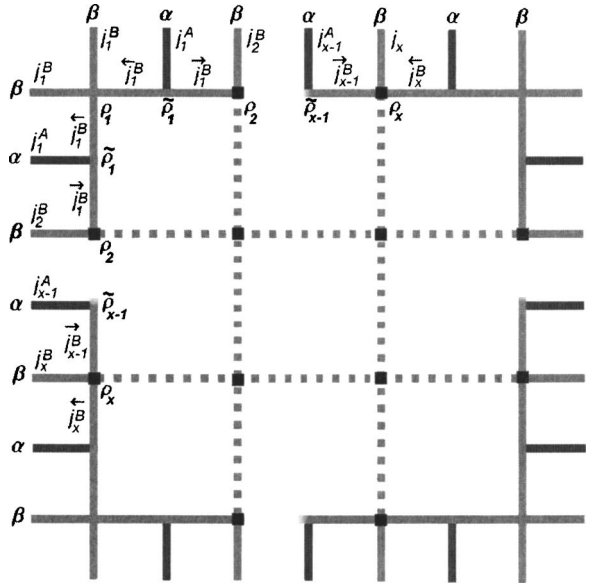

FIG. 9. Reduced system for the case of fast reactivity. The symmetry of the problem is included in the notation.

$$j_x^B = D\frac{\rho_x}{L+1}. \tag{2}$$

Here, ρ_x is the product particle density at intersection x connected to the β segment. The derivation of the currents involves a simplification. Within a mean field approximation, joint probabilities $\langle xy\rangle$ of particle numbers between an intersection and its adjacent sites can be replaced by the product of the individual averages $\langle x\rangle\langle y\rangle$. This well controlled approximation is, in fact, necessary only in the vicinity of intersections, since any joint probability vanishes in the bulk of the channels.[20] The expected relative error is of the order of $1/L$.[18,22] Reactant particles diffuse into the system through α segments which are bounded at one side by the reservoir (density ρ_A) and at the other side by intersection $\tilde{\rho}_x$ with current

$$j_x^A = D\frac{\rho_A(\tilde{\rho}_x - 1)}{L(\tilde{\rho}_x - 1) - 1}. \tag{3}$$

Finally, the intrinsic currents, determined by two adjacent intersections follow to

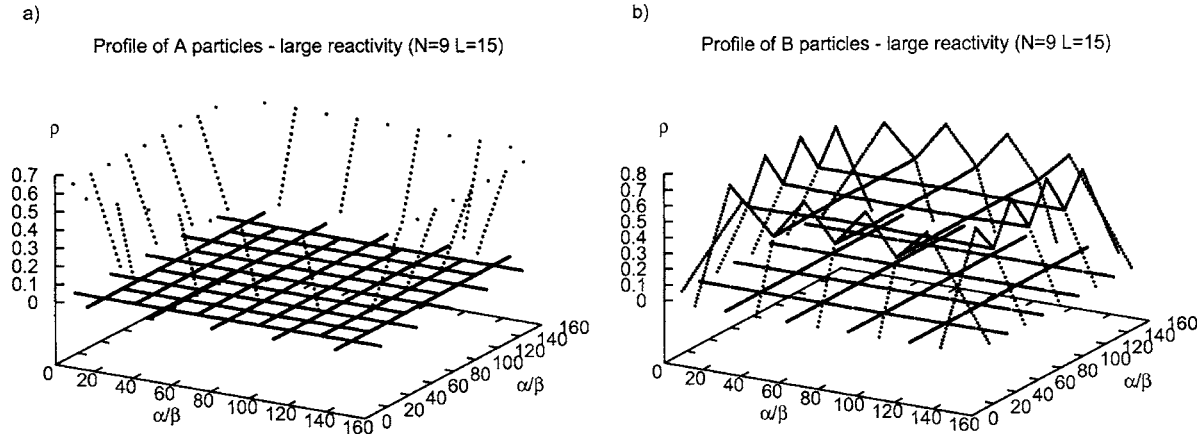

FIG. 8. A/B particle profile (a)/(b) for a system of $N=9$, $L=15$ and reactivity $c=1000$.

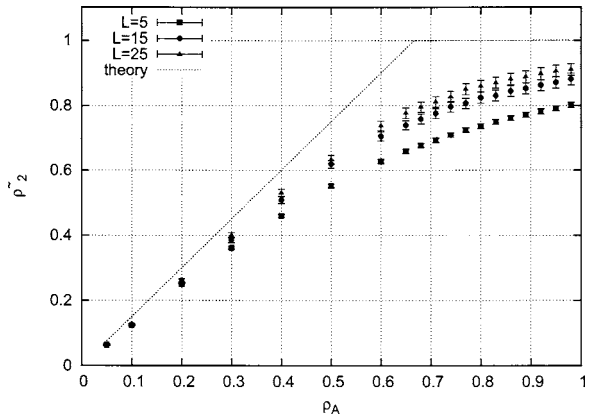

FIG. 10. Density $\tilde{\rho}_2$ for different L as a function of the reservoir density. The theoretical density is indicated by the dotted line. $N=9$.

$$\overleftarrow{j}_x^B = D\frac{\tilde{\rho}_x - \rho_x}{L+1}, \tag{4}$$

$$\vec{j}_x^B = D\frac{\tilde{\rho}_x - \rho_{x+1}}{L+1}. \tag{5}$$

The arrows are not supposed to indicate vectors but to distinguish the direction of currents in order to comply with the zigzag profile shown in Fig. 8.

Making use of the conservation of currents,

$$j_x^A = \overleftarrow{j}_x^B + \vec{j}_x^B, \tag{6}$$

$$j_x^B = \overleftarrow{j}_x^B + \vec{j}_{x-1}^B, \tag{7}$$

we find (for large but finite L) two coupled recursion relations for the intersection densities which determines the density profile.

$$\tilde{\rho}_x = \begin{cases} 1 \\ \frac{1}{2}(\rho_x + \rho_{x+1} + \rho_A), \end{cases} \tag{8}$$

$$3\rho_x = \tilde{\rho}_x + \tilde{\rho}_{x+1}. \tag{9}$$

Let $N_\alpha = [N/2]$ be the number of α channels. In order to ensure zero current in the equilibrium parts of the β channels (Fig. 9), intersections marked with a black square need to attain equal density. Hence, in the region $2 \leqslant x \leqslant N_\alpha$ we assume a constant solution for the densities ρ_x and find $\rho_x \equiv \rho = \rho_A$. Intersections $\tilde{\rho}_x$ connected to α channels carry a product particle density 3/2 times higher (Fig. 10) and therefore $\tilde{\rho}_x \equiv \tilde{\rho} = 3/2\rho_A$. Since the particle density cannot exceed 1, ρ saturates for a boundary density of $\rho_A = 2/3$. This has an intersecting consequence. Changing the boundary density from $\rho_A = 2/3$ to $\rho_A = 1$ merely shifts up the profile of the α channels; the output, however, keeps unchanged. For the sake of completeness we remark that for the four corners $2\rho_1 = \tilde{\rho}_1$, hence, $3\rho_1 = 2\rho_A$.

We have now determined the profile. Because of (2) the output of product particles for each β channel is independent of the number of channels; hence, the total output current scales linearly with N. Figure 10(a) shows the profile of intersection $\tilde{\rho}_2$ as a function of the reservoir density for a system of $N=9$ channels and different L. The saturation at $\rho_A = 2/3$ predicted for $L \to \infty$ (vanishing corrections to mean field theory) becomes more pronounced for increasing L. The theoretical description is good for small reservoir densities. The largest deviation (about 20% at most) occurs for the predicted saturation point, so for practical purposes the theoretical analysis agrees well with the simulated data.

V. MTC MODEL WITH SIZE SELECTIVITY

For situations where channel selectivity merely originates from different pore diameters we have to modify our model. Consider the model shown in Fig. 1 but now allowing reactant as well as product particles to diffuse along the α channels (size selectivity). We call them γ channels. Assuming β channels to be smaller in diameter than α channels, there is no reason why particles of type B would avoid occupying α-channels. Of course, we could also consider the situation vice versa, with β being larger than α. However, this leads to a reduction of output channels; hence, this situation would be counterproductive and is not studied here. Overtaking is still prohibited for any type of particles. The dynamics explained in the Model section remains unchanged. Similar to arguments given before we would like to

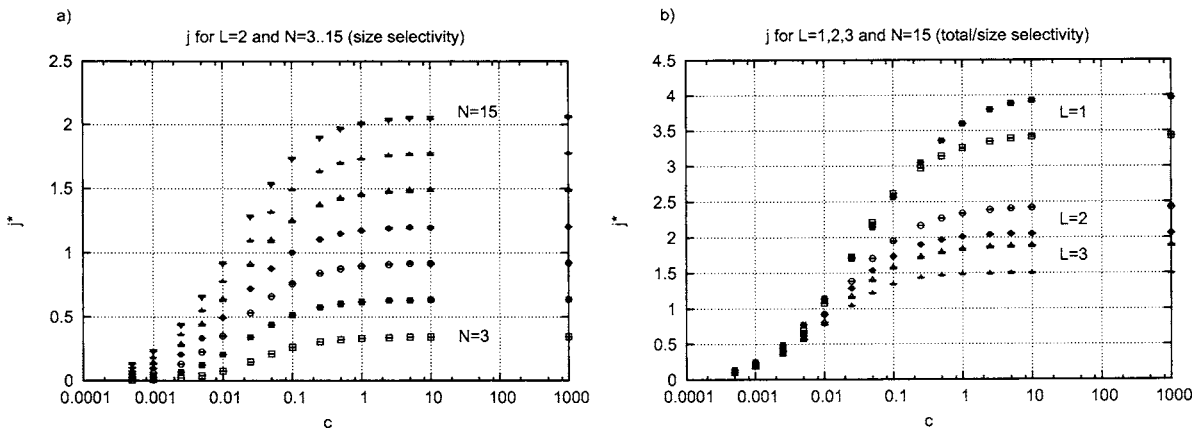

FIG. 11. (a) Maximal currents j^* over reactivity c for the size controlled MTC system. (b) Maximal Currents for the size controlled system (solid symbols) and the system of total selectivity (open symbols).

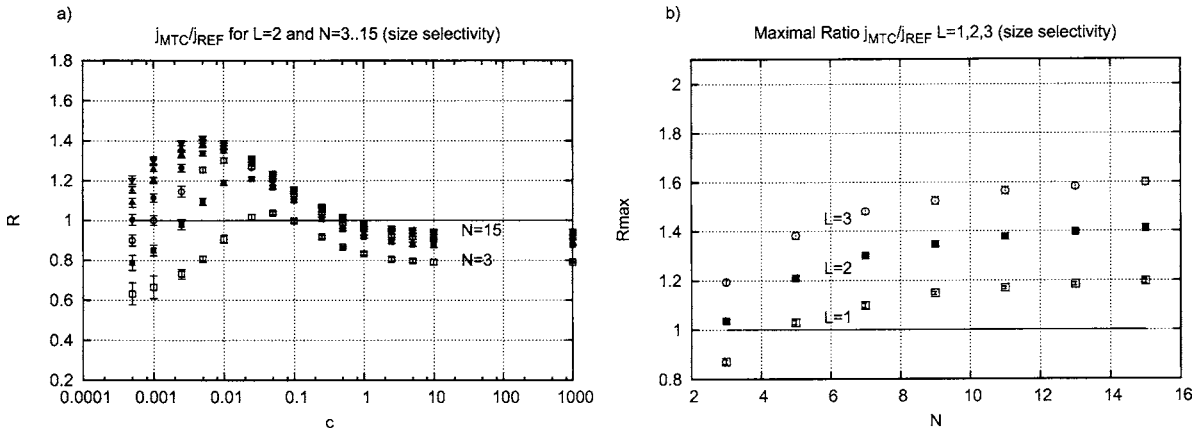

FIG. 12. (a) Ratio $R(c)$ for different number of channels N and $L=2$. (b) Maximal ratio R^* for different L (size selectivity).

compare it with the REF system for equal internal parameters (N,L,c) but in their maximal current state with respect to the reservoir density ρ_A.

Comparing the currents of the size-controlled system [Fig. 11(a)] with the model of total selectivity [Fig. 5(a)], we find a similar qualitative behavior. There is an interesting observation that the size-controlled model perform a higher output compared to the model of total selectivity for $L=1$; however, for larger L total selectivity becomes more and more efficient (Fig. 11(b)). This is true for high enough reactivities. Both models maximize their output for infinite reactivity; hence, both models are surface active in their state of maximal performance, since for large reactivities the interior becomes rather inactive due to lacking particles of type A. The efficiency R is plotted in Fig. 12(a) for $L=2$. Similar to the case of total selectivity [Fig. 6(a)], R undergoes a maximum for some intermediate c; however, we observe a shift to smaller reactivities. Plotting the maximal efficiency for increasing N [Fig. 6(b)] proves the fact that the MTC effect is present for any L.

VI. CONCLUSION

Our simulations and analytical results describe the MTC effect quantitatively over a wide range of parameters for a model of alternating α and β channels and novel channel topology. The output current scales linearly with the number of channels and, hence, the efficiency ratio (compared with a topologically and structurally similar reference system without MTC) does not sharply decrease with increasing system size. This new insight is encouraging as it allows for the MTC effect in experimental settings not only for nanoscale systems. This suggests that MTC may enhance significantly the effective reactivity in zeolitic particles with suitable binary channel systems and thus may be of practical relevance in applications. Introducing a model of size selectivity where reactant as well as product particles are allowed to enter α channels reveals only minor differences in the observed behavior. For the important case of small channel segments, size selectivity seems to be slightly more efficient compared to total selectivity.

ACKNOWLEDGMENTS

Financial support by the Deutsche Forschungsgemeinschaft is gratefully acknowledged. We also thank Jörg Kärger and Peter Bräuer for useful discussions.

[1] Ch. Baerlocher, W. M. Meier, and D. H. Olson, *Atlas of Zeolite Structure Types* (Elsevier, London, 2001).
[2] J. Kärger and D. M. Ruthven, *Diffusion in Zeolites and Other Microporous Solids* (Wiley, New York, 1992).
[3] E. G. Derouane and Z. Gabelica, J. Catal. **65**, 486 (1980).
[4] E. G. Derouane, Appl. Catal., A **115**, N2 (1994).
[5] R. Q. Snurr and J. Kärger, J. Phys. Chem. B **101**, 6469 (1997).
[6] L. A. Clark, G. T. Ye, and R. Q. Snurr, Phys. Rev. Lett. **84**, 2893 (2000).
[7] L. A. Clark, A. Gupta, and R. Q. Snurr, J. Phys. Chem. B **102**, 6720 (1998).
[8] N. Neugebauer, P. Bräuer, and J. Kärger, J. Catal. **194**, 1 (2000).
[9] J. Kärger, P. Bräuer, and H. Pfeifer, Z. Phys. Chem. (Munich) **104**, 1707 (2000).
[10] J. Kärger, P. Bräuer, and A. Neugebauer, Europhys. Lett. **53**, 8 (2001).
[11] P. Bräuer, A. Brzank, and J. Kärger, J. Phys. Chem. B **107**, 1821 (2003).
[12] A. Brzank, G. M. Schütz, P. Bräuer, and J. Kärger, Phys. Rev. E **69**, 031102 (2004).
[13] A. Brzank and G. M. Schütz, Appl. Catal., A **288**, 194 (2005).
[14] A. Brzank, S. Kwon, and G. M. Schütz, Diffusion Fundamentals **1**, 1 (2005).
[15] J. S. Beck, J. C. Vartulli, W. J. Roth *et al.*, J. Am. Chem. Soc. **114**, 10834 (1992).
[16] J. H. Sun, Z. Shan, Th. Maschmeyer, and M.-O. Coppens, Langmuir **19**, 8395 (2003).
[17] F. Spitzer, Adv. Math. **5**, 246 (1970).
[18] H. Spohn, J. Phys. A **16**, 4275 (1983).
[19] H. van Beijeren, K. W. Kehr, and R. Kutner, Phys. Rev. B **28**, 5711 (1983).
[20] G. Schütz and S. Sandow, Phys. Rev. E **49**, 2726 (1994).
[21] T. M. Liggett, *Stochastic Interacting Systems: Contact, Voter and Exclusion Processes* (Springer, Berlin, 1999).
[22] G. M. Schütz, in *Phase Transitions and Critical Phenomena*, edited by C. Domb and J. Lebowitz (Academic, London, 2001).
[23] C. Rödenbeck and J. Kärger, J. Chem. Phys. **110**, 3970 (1999).